

Transient creep analytical modeling for shear endplate assemblies in fire

Hadi O. Al Haddad and Elie G. Hantouche
*Department of Civil and Environmental Engineering,
American University of Beirut, Beirut, Lebanon*

Transient
creep
analytical
modeling

289

Received 22 August 2019
Revised 11 November 2019
Accepted 9 January 2020

Abstract

Purpose – The purpose of this study is to develop an analytical model that is capable of predicting the behavior of shear endplate beam-column assemblies when exposed to fire, taking into account the thermal creep effect.

Design/methodology/approach – An analytical model is developed and validated against finite element (FE) models previously validated against experimental tests in the literature. Major material and geometrical parameters are incorporated in the analysis to investigate their influence on the overall response of the shear endplate assembly in fire events.

Findings – The analytical model can predict the induced axial forces and deflections of the assembly. The results show that when creep effect is considered explicitly in the analysis, the beam undergoes excessive deformation. This deformation needs to be taken into account in the design. The results show the significance of thermal creep effect on the behavior of the shear endplate assembly as exposed to various fire scenarios.

Research limitations/implications – However, the user-defined constants of the creep equations cannot be applied to other connection types. These constants are limited to shear endplate connections having the material and geometrical parameters specified in this study.

Originality/value – The importance of the analytical model is that it provides a time-effective, simple and comprehensive technique that can be used as an alternative to the experimental tests and numerical methods. Also, it can be used to develop a design procedure that accounts for the transient thermal creep behavior of steel connections in real fire.

Keywords Shear endplate assembly, Transient state, Creep, Analytical model

Paper type Research paper

1. Introduction

Common practices of structural design of steel beam-column assemblies classify connections as simple, rigid or semi-rigid connections. Specifically, the shear endplate connection is considered a simple connection because of its high rotational ductility. However, when the steel column-beam assembly is exposed to fire, the beam induces axial forces. These forces are initially compressive up to the point where significant catenary action might initiate in the beam, which generates tensile forces at the end of heating and in the cooling phase. The induced axial forces and the excessive deformations accompanied with stiffness and strength degradations of the connection might lead to the total collapse of the structure. The prediction of the thermal response of the column-beam assembly becomes more complex if time-dependent or the so-called creep effect is included. Therefore, this paper provides a simplified analysis of the transient thermal creep behavior of steel column-beam assemblies when subjected to different fire scenarios.

Several attempts to study the behavior of shear endplate connections in fire have been conducted. One of those methods is the so-called mechanical modeling (or stiffness-based



method). It begins by assigning each active structural component with a stiffness or a spring, and then assembles these springs in a certain manner to predict the real behavior of the assembly (Jaspart *et al.*, 1995). Based on the mechanical models proposed (Spyrou *et al.*, 2004; Al-Jabri *et al.*, 2005; Block, 2006; Sarraj, 2007), a mechanical model of the isolated shear endplate connection was performed by Hu *et al.* (2009). Shear, tension and rotation behavior were modeled by Hu *et al.* (2009) by including shear, weld, bolt and endplate springs and neglecting the column behavior. Moreover, Hantouche and Sleiman (2017) used finite element (FE) models to investigate different parameters affecting isolated shear endplate connections, and then proposed a mechanical model excluding the creep effect to estimate the behavior of shear endplates under fire loads. However, none of the mechanical models presented included any thermal creep behavior, which disagrees with recent studies that emphasize the time-dependent behavior in steel structures (Kodur and Dwaikat, 2010; Yang and Yu, 2013).

The tendency of solid materials to deform slowly over time under both elevated temperatures and stresses is defined as the thermal creep. Thermal creep is more severe as the material temperatures approach its melting point. In fact, thermal creep of steel is highly dependent on steel material type, loads, temperatures and time durations. Thermal creep of steel is represented in a creep strain versus time curves and comprised of three phases. The first phase is the primary phase where the creep strain is increasing at a decreasing rate. In the secondary phase, the creep strain increases at a steady-state rate, whereas it increases rapidly with time in the tertiary stage until the material fractures.

The importance of thermal creep has been recognized in steel structures (Kodur and Dwaikat, 2010; Yang and Yu, 2013). These studies revealed that during a fire, the steel behavior is highly dependent on stresses, fire exposure durations and temperature levels. For instance, Kodur and Dwaikat (2010) included the thermal creep explicitly in the FE simulations using Harmathy (1967) and ANSYS creep models. The beam was modeled by replacing its ends with axial and rotational springs having stiffnesses not accounting for the column height. The results show that the thermal creep helps in providing accurate predictions of unrestrained beam deflection as well as restrained beam axial force. Further, SN490FR fire-resistant steel was extensively studied by Yang and Yu (2013), who observed that the column buckling temperatures were changing with time, depending on the level of column restraint. Recently, Jabotian and Hantouche (2018) conducted a series of FE parametric studies to study the thermal creep behavior of isolated shear tab connections in fire. The results show that the shear tab connection experienced different failure modes, additional rotations and displacements when thermal creep effect was included. In addition, the National Institute of Standard and Technology (NIST) considered the thermal creep in columns and floor trusses of all simulations of the WTC building collapse that occurred on September 11, 2001 (Luecke *et al.*, 2005).

The thermal creep effect can be included using two methods: implicit and explicit models. The implicit creep model includes the creep in the material stress–strain properties, while the explicit creep model adds the computed creep strains to the mechanical strains (Torić *et al.*, 2013). The implicit consideration of thermal creep is considered conservative when the same material is subjected to longer fire durations (Kodur and Dwaikat, 2010).

Inclusion of the thermal creep effect in mechanical modeling is limited due to its complexity. Few mechanical models were developed to predict the time-dependent response in different types of connections and materials at elevated temperatures. Torić and Burgess (2016) proposed a unified mechanical model that was able to predict the creep strains in S275 and S355 steel materials subjected to both steady- and transient-state thermal conditions. The model was based on the Eurocode 3 (2005) and composed of several Kelvin–Voigt models connected in series to validate various stress and strain-rate controlled tests.

Moreover, [El Ghor and Hantouche \(2017\)](#) developed a mechanical model to predict explicitly the time-dependent creep behavior of isolated flush endplate connections. It should be noted that the flush endplate connections studied were isolated, which means that only the local contributions of the column (flange in bending, web in shear, tension and compression) were included, rather than the effect of the column stiffness as an element (i.e. column height). Further to the limited mechanical models including time-dependent behavior, very limited work on the full-scale transient behavior of steel assemblies, including time-dependent parameters, was studied.

Analytical modeling consists of mathematical equations that have a closed-form solution. In this study, the assembly is divided into the beam, unheated and heated column and endplate. Based on each element's geometry and material, the stiffness for each element is calculated. As two-dimensional frame elements are defined by three degrees of freedom at each of their start and end node, the stiffness of the element is represented by a 6×6 stiffness matrix. The stiffness matrices for all of the elements are then joined to form a global stiffness matrix of the assembly. This global stiffness is used to compute the forces and displacements of the assembly at each temperature increment. Thermal creep is introduced to the analytical model directly by the means of creep strain formulas from existing material creep models.

This study proposes a simplified analytical model that includes the transient-state creep effect for various key parameters of shear endplate assemblies under fire loads. FE models are first developed in [ABAQUS \(2014\)](#) and validated against the experimental work done at the University of Manchester by [Wang *et al.* \(2011\)](#). Then, the effect of key parameters such as the heating and cooling rates, initial cooling temperatures, load ratios and column heights and sizes are investigated while including and excluding thermal creep effect ([Al Haddad *et al.*, 2019](#)). Then, an analytical model is developed to analyze the assembly for all aforementioned parameters for different fire scenarios. The beam axial force and mid-span deflection are predicted using the analytical model and compared with the FE results. This research shows that a simplified fire analysis of the assembly can be achieved by the proposed analytical model with reasonable accuracy. Further, as disregarding creep may lead to unsafe design of steel structures exposed to elevated temperatures, including creep in designing shear endplate connections in fire is necessary.

2. Constitutive creep models

Regarding creep in different steel materials, extensive research has been performed ([Harmathy, 1967](#); [Fields and Fields, 1989](#); [Morovat, 2014](#); [Wang *et al.*, 2017](#)). In the empirical Fields and Fields creep model (1989), the creep strain, ε_c , is represented using a Norton–Bailey (power-law) equation as shown:

$$\varepsilon_c = at^b \sigma^c \quad (1)$$

where t is the time in minutes; σ is the stress in ksi; and a , b , and c are material- and temperature-dependent parameters. The Fields and Fields model can predict thermal creep up to 6% creep strains within 350–600°C temperatures. Note that this model only predicts the primary and secondary stages of a creep curve. As the tertiary stage cannot be modeled using the presented creep model, it was not included in this research.

It should be noted that the creep subroutine used in the FE simulations of this study is based on the subroutine proposed and validated by [Hantouche *et al.* \(2018\)](#). Based on Fields and Fields model, the authors were able to calculate creep strains in FE models explicitly. At the beginning of each increment, the subroutine estimates the changes in the creep strain. These changes are based on the creep strain history, instant temperatures and stresses for

every mesh element in the ABAQUS model by assuming constant conditions in each increment. However, the original subroutine was not able to include the creep behavior in materials other than S275. Thus, in the FE simulations conducted in this study, the user-defined subroutine is modified to allow for including creep in two different materials: S275 for the beam and endplate and S355 for the column. Thus, the creep was not included in the bolts and welds of the FE simulations.

For considering thermal creep in other steel grades, a modification to [equation \(1\)](#) was proposed by [Luecke *et al.* \(2005\)](#). It was observed that the yield strength follows a universal curve when normalized to their ambient temperature values. Hence, when applying a certain scale by yield strength ratios, A36 steel creep models can be used to predict the creep strains in S275 and S355 grades as follows:

$$\sigma_c = R_\sigma \sigma_a \quad (2)$$

where R_σ is the relative ratio of the yield strength of A36 steel to the untested steel material, and σ_a is the applied stress. As Eurocode steel S275 has the same yield strength as that of American steel A36, this equation was not needed to be modified in the ABAQUS subroutine. On the other hand, the yield stresses of S355 and A36 are not the same. Hence, [equation \(2\)](#) was used to compute the corrected stress and include it in [equation \(1\)](#).

3. Finite element modeling

For reproducing the fire experiments performed at the University of Manchester ([Wang *et al.*, 2011](#)), ABAQUS was used to model the FE simulations of shear endplate assemblies. Further to the validation purposes, parametric studies on the shear endplate assemblies were also developed. The parameters covered in the FE simulations were heating and cooling rates, initial cooling temperatures, column sizes and heights, load ratios, plate thicknesses and steel grades. More detailed discussions on the FE validations and simulations can be found in [Al Haddad *et al.* \(2019\)](#).

Two of the fire experiments consisted of shear endplate connections, which are Tests 2 and 7 in [Wang *et al.* \(2011\)](#). Both tests share the same beam section (UB 178 × 102 × 19) having a length of 2 m connected by a 150 × 130 × 8 mm shear endplate, to two columns having a height of 3.67 m. Column sections UC 254 × 254 × 73 and UC 152 × 152 × 23 were used in Tests 2 and 7, respectively. Geometrical details representing the full-scale assembly of the shear endplate tests are shown in [Figure 1](#).

The large columns of Test 2 were made from Grade S355 steel, while the beam, shear endplate and the small columns of Test 7 were made from Grade S275 steel. Nonetheless, [Wang *et al.* \(2011\)](#) performed tensile coupon tests on the tested elements, which showed a slight increase in the mechanical properties of S275 and S355 steel grades. In addition, the bolts and nuts in the connection were of Grade 8.8 steel in all tests. The retention factors proposed by [Lee *et al.* \(2013\)](#) and [Hu *et al.* \(2007\)](#) were used for both the structural steel and bolts, respectively. [Figure 2](#) represents the elastic modulus retention factors used in the base material of this study based on the research done by [Lee *et al.* \(2013\)](#).

Only half of the frame was modeled with an applied symmetric condition at the beam mid-span section, because the assembly in the experiment was designed to be symmetric about the mid-span section of the beam. First, pre-tensioning of the four bolts was assigned in all FE simulations. Then, a 0.5 load ratio, represented by a 40 kN gravity load was distributed over the load jacks' area 600 mm away from the connection. Following the loading stage, the heating stage comprised heating all steel components except for the top

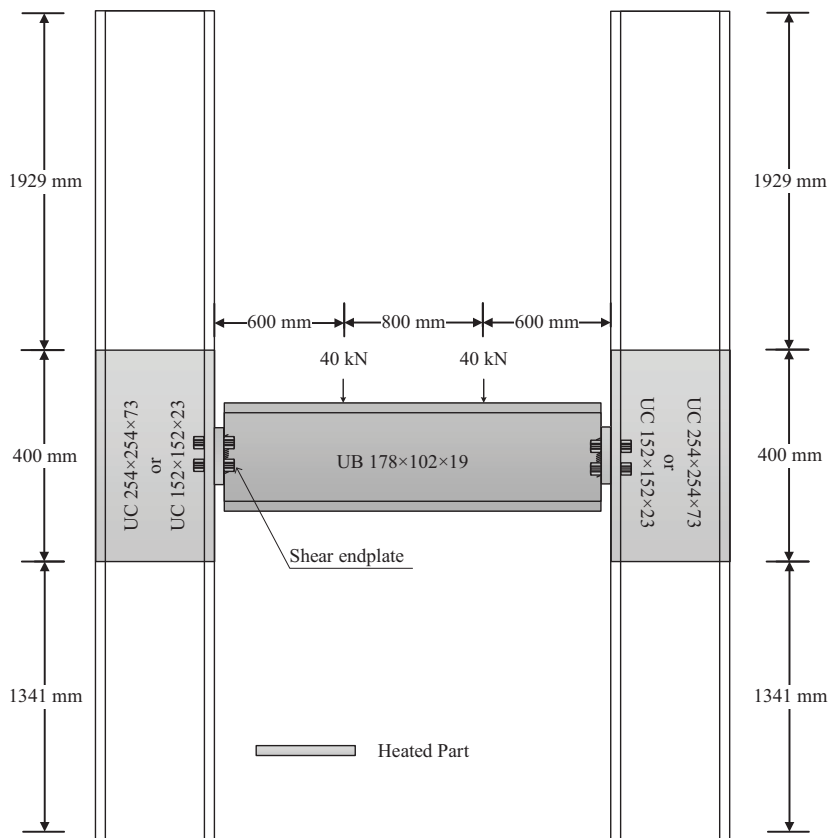


Figure 1. Details of the fire tests on the steel frame assembly of Wang *et al.* (2011)

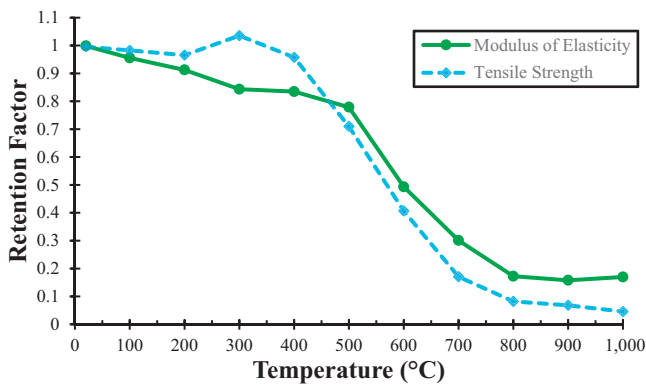


Figure 2. Modulus of elasticity and tensile strength retention factors (Lee *et al.*, 2013)

and bottom of the column from ambient temperatures, then cooling back to ambient conditions in the final cooling stage.

All column ends were restrained from horizontal displacement. Additionally, the lower column ends were restrained from moving vertically. A tie constraint joining the shear endplate and the beam was used to model the weld. Moreover, to represent the restraining action of the concrete slab on the beam top flange, the latter was assigned a lateral displacement restriction.

The test consisting of shear endplate connections faced difficulties maintaining the same temperature throughout the heating of members inside the furnace (Wang *et al.*, 2011). Therefore, it was necessary to account for temperature non-uniformity in the FE assembly by dividing it to six parts classified by their temperature levels. The part with the highest temperature is the beam bottom flange followed by the beam web, connection area, beam upper flange, heated column panel zone (400 mm) and the remaining unheated column parts.

4. Analytical modeling

The proposed analytical model method is discussed in this section. The first step of the model is explained in terms of user inputs and stiffness computations. Then, details of the methodology used in both fast and creep analyses are discussed.

4.1 User inputs

The first set of inputs required is the material set, which covers the modulus of elasticity; thermal expansion coefficients; and the yield strengths for each of the beam, column and shear endplate. The material used is based on retention factors proposed by Lee *et al.* (2013). The second input set is the nodes of the assembly, which can be entered in any order. The nodes set consists of the point loads, boundary conditions and nodal coordinates following the global x-y-z axes. The third set is the elements properties, which are the end nodes, sectional areas, moments of inertia, depths and loads between the nodes following the local axes of each member. The last set is the thermal analysis that is concerned with the maximum heating temperature, the heating and cooling increments and the selection of fast or creep analysis.

4.2 Element stiffness

The stiffness, K , of a beam element, i , having a modulus of elasticity, E , a cross-sectional area, A , moment of inertia, I , and a length, L , is defined in the beam stiffness matrix as shown below:

$$K_i = \begin{bmatrix} \frac{E_i A_i}{L_i} & 0 & 0 & -\frac{E_i A_i}{L_i} & 0 & 0 \\ 0 & \frac{12E_i I_i}{L_i^3} & \frac{6E_i I_i}{L_i^2} & 0 & -\frac{12E_i I_i}{L_i^3} & \frac{6E_i I_i}{L_i^2} \\ 0 & \frac{6E_i I_i}{L_i^2} & \frac{4E_i I_i}{L_i} & 0 & -\frac{6E_i I_i}{L_i^2} & \frac{2E_i I_i}{L_i} \\ -\frac{E_i A_i}{L_i} & 0 & 0 & \frac{E_i A_i}{L_i} & 0 & 0 \\ 0 & -\frac{12E_i I_i}{L_i^3} & -\frac{6E_i I_i}{L_i^2} & 0 & \frac{12E_i I_i}{L_i^3} & -\frac{6E_i I_i}{L_i^2} \\ 0 & \frac{6E_i I_i}{L_i^2} & \frac{2E_i I_i}{L_i} & 0 & -\frac{6E_i I_i}{L_i^2} & \frac{4E_i I_i}{L_i} \end{bmatrix} \quad (3)$$

Note that the stiffness presented assumes no shear deformation in the elements. This assumption is acceptable when the element is not short enough to deform in shear. Hence, shear deformation effects were mainly observed in the short column element when column length was analyzed. The shear deformation constant, β , can be written as shown:

$$\beta = \frac{12EI f_s}{GAL^2} \tag{4}$$

where f_s is the shape factor taken 1 for the case of wide flange beams bending about the major axis, and G is the shear modulus of the steel material. The stiffnesses of all elements are assembled to form a global stiffness, K . This stiffness is used in the below equation to compute the internal forces from the displacements and fixed end forces (FEF):

$$\begin{bmatrix} F_{x1} \\ F_{y1} \\ M_1 \\ F_{x2} \\ F_{y2} \\ M_2 \end{bmatrix} = K \begin{bmatrix} x_1 \\ y_1 \\ \theta_1 \\ x_2 \\ y_2 \\ \theta_2 \end{bmatrix} + FEF \tag{5}$$

The matrix multiplied by K is the deflection matrix; the product is used to compute the internal force matrix shown on the left-hand side of equation (5). F_x , F_y and M are the axial force, major shear and major bending moment, respectively. x , y and Θ are the axial displacement, lateral deflection and rotation, respectively. Subscript 1 denotes the beam extremity closer to the connection, whereas subscript 2 denotes the symmetry side.

The elements in the proposed model are divided into two unheated column parts of different heights, a heated column part in between, a shear endplate element and the half of a beam. All the elements discussed represent the left-hand side of the assembly with a symmetry condition preventing rotation and axial deformation at the beam mid-span, as shown in Figure 3. To provide better deflection results, the rotational stiffness of the shear endplate, K_{con} , is used. This stiffness is based on the rotational stiffness proposed by Hantouche *et al.* (2018) for double angle and shear tab connections as shown:

$$K_r = K_e h^2 \tag{6}$$

where K_r and K_e are the connection rotational and axial stiffnesses, respectively, and h is the distance between the end components of the connection and the column connected. The rotational stiffness in equation (6) can be written as follows:

$$K_{con(t)} = \frac{\Omega E_{p(t)} A_{p(t)} h_p^2}{t_p} \tag{7}$$

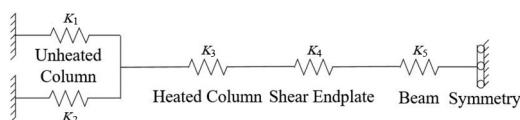


Figure 3.
Modeling
components of the
frame

where $E_{p(t)}$, $A_{p(t)}$, h_p and t_p represent at a given time, the elastic modulus, cross section area, height, and thickness of the plate, respectively. To apply the stiffness equation proposed by [Hantouche et al. \(2018\)](#) for double angle and shear tab connections on shear endplate connections, a correction factor, Ω , is introduced to ensure the accuracy of the rotational stiffness computation. The value of this factor was estimated based on changing the geometrical properties of the shear endplate and computing the connection rotations and moments for each case with the help of FE models. Based on this proposed estimation, the value of 0.0001 was used providing a reasonable accuracy of the connection stiffness. Further, the beam moment, M , at the connection end can be computed from the connection rotation, Θ_{con} :

$$M = K_{con(t)} \theta_{con} \tag{8}$$

Therefore, implementing [equation \(8\)](#) in the third row of the beam stiffness matrix shown in [equation \(3\)](#) leads to the following change in the stiffness, K :

$$K = \frac{EI}{zL^3(1 + \beta)}$$

$$\times \begin{bmatrix} \frac{zAL^2(1 + \beta)}{I} & 0 & 0 & -\frac{zAL^2(1 + \beta)}{I} & 0 & 0 \\ 0 & 12(z - 3EI) & 0 & 0 & -12(z - 3EI) & 6L[z - (2 - \beta)EI] \\ 0 & 0 & \frac{K_{con}zL^3(1 + \beta)}{EI} & 0 & 0 & 0 \\ -\frac{zAL^2(1 + \beta)}{I} & 0 & 0 & \frac{zAL^2(1 + \beta)}{I} & 0 & 0 \\ 0 & -12(z - 3EI) & 0 & 0 & 12(z - 3EI) & -6L[z - (2 - \beta)EI] \\ 0 & 6L[z - (2 - \beta)EI] & 0 & 0 & -6L[z - (2 - \beta)EI] & L^2[z(4 + \beta) - (2 - \beta)^2EI] \end{bmatrix} \tag{9}$$

where the factor z can be calculated as follows:

$$z = EI(4 + \beta) + K_{con}L(1 + \beta) \tag{10}$$

The FEF are also updated following the implementation of [equation \(8\)](#) in the stiffness, K :

$$FEF = \begin{bmatrix} F_{x1}^F \\ F_{y1}^F - \frac{6EIM_1^F}{zL} \\ 0 \\ F_{x2}^F \\ F_{y2}^F + \frac{6EIM_1^F}{zL} \\ M_2^F - \frac{(2 - \beta)EIM_1^F}{z} \end{bmatrix} \tag{11}$$

Superscript F denotes the FEF or moment, which is computed based on the load characteristics between two nodes. The connection rotation can be computed as follows:

$$\theta_{con} = \frac{EI(4 + \beta)}{z} \left[\frac{6(y_2 - y_1)}{L(4 + \beta)} - \frac{\theta_2(2 - \beta)}{(4 + \beta)} - \frac{M_2^F L(1 + \beta)}{EI(4 + \beta)} \right] \quad (12)$$

4.3 Fast analysis

The procedures of both the fast and creep analyses are summarized in Figure 4. At a given time (t) and temperature (T), displacements of all free nodes of the assembly, except for the connection rotation, are computed. The incremental axial forces, ΔP , and moments, ΔM , are computed using the global stiffness matrices. Then, the connection rotation is computed using equation (12). The incremental axial force, ΔP , at a specified time, t , is added to the total axial force in the previous time increment to compute the beam axial force at the end of the increment as shown:

$$P_{(t)} = P_{(t-1)} + \Delta P \quad (13)$$

The moments generated at the end of each time are computed with the addition of constants c_1 , c_2 and c_3 as shown below:

$$M_{(t)} = M_{(t-1)} c_{1,2,3}^{\frac{\Delta T}{T_0}} + \Delta M \quad (14)$$

Only one of the constants is used at each temperature depending on the temperature range. The constants shown in Table 1 represent the temperatures in the cooling phase higher than 500, 400 and 20, for different analytical model cases. The main function of such constants is to take into account the catenary action effects that initiate at the end of the heating phase in the beam. The catenary effect applies to any system where significant tension is generated by transverse loads on an element with restrained ends. As represented in Figure 5, the P - Δ effect provides additional moments that in turn tend to reduce the deflection.

The last stage in the fast analysis is to calculate the mid-span deflection, $\Delta_{(t)}$. This can be achieved by computing the connection rotation. The connection rotation is computed from its rotational stiffness, $K_{con(t)}$, and moment, $M_{(t)}$, at a certain time, t . The adjusted length, L_{adj} , is the average of the distances from the connection to the point load and mid-span, which is 800 mm in this assembly. The below equation was validated on a flush endplate connection as well and proved reasonably accurate when computing deflections for all analytical model cases presented in this study:

$$\Delta_{(t)} = \frac{M_{(t)} L_{adj}}{K_{con(t)}} \quad (15)$$

Internal stresses exceeding the material yielding strength are most likely to occur in the beam and endplate when subjected to fire loads. In addition, as the portion of yielded area cannot be precisely computed from the analytical model, a 1% area reduction is assumed. The area reduction is applied to the area in the previous time increment to compute the area in the current time increment. This reduction is applied to the element's cross-sectional area whenever its von Mises stress, σ_v , exceeds the material yielding strength at a certain time or temperature:

$$\sigma_v = \sqrt{\frac{(\sigma_x - \sigma_y)^2 + (\sigma_x - \sigma_z)^2 + (\sigma_y - \sigma_z)^2}{2}} + 3(\tau_{xy}^2 + \tau_{xz}^2 + \tau_{yz}^2) \quad (16)$$

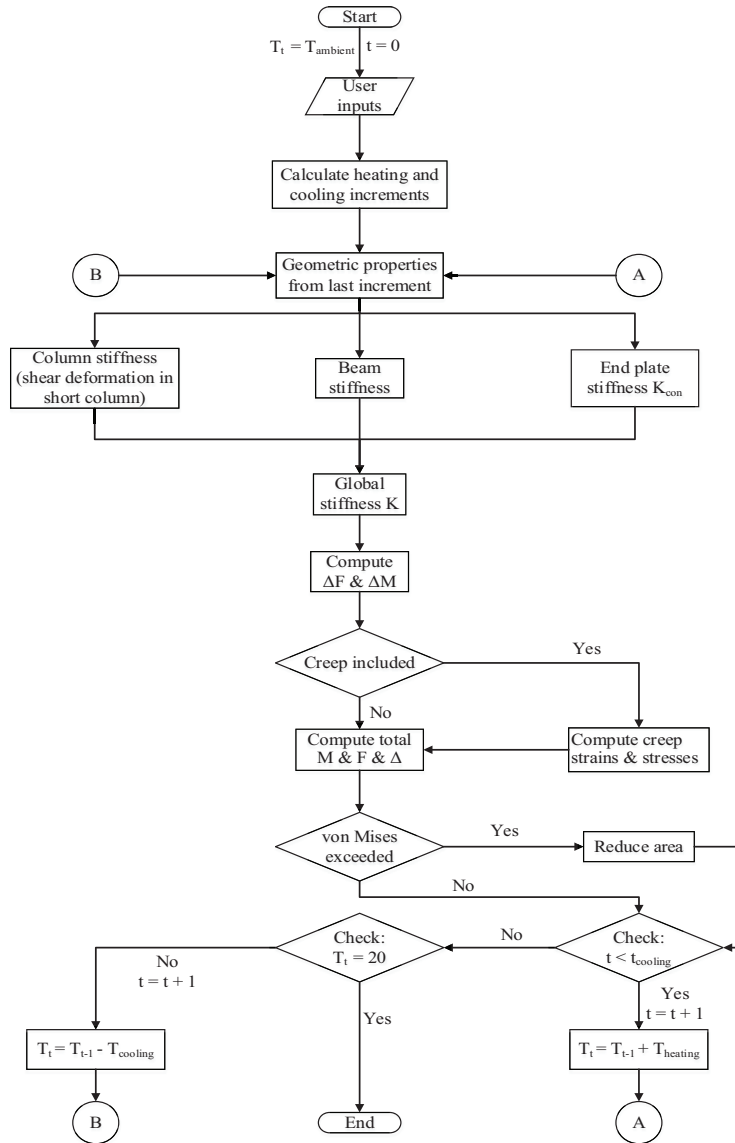


Figure 4. Flowchart of the incremental time-dependent analytical model of shear endplate connection

The axial stress, σ_x , is taken at the most stressed points in the section, which are the upper and lower extremities taking into account the moment and axial forces directions. The shear stress, τ_{xy} , is calculated on all points except for the mid-span of the beam where it is theoretically zero.

4.4 Creep analysis

The creep analysis is active only when two conditions are met; the creep analysis is permitted by the user, and the temperature is within the 350–600°C range. This range is based on the limitation

of the [Fields and Fields \(1989\)](#) creep model used in the FE models ([Al Haddad et al., 2019](#)). As the analytical model uses the same creep model to validate the FE models, the maximum temperature encountered in the analytical model is 600°C. The creep analysis follows the same procedure as the fast analysis, with a few additional steps. The proposed method includes creep by relying completely on creep equations embedded in the code with the help of user-defined constants applied at each increment. The proposed creep constants are tested on the model for all parameters, which leads to enhancing the accuracy of the analytical model. All parameters in this section refer to the beam mid-span section where beam axial forces and deflections are predicted. An approximate axial stress, $\sigma_{(t)}$, is computed using the last axial force generated from the fast analysis divided by the area of the beam at a certain time, t , as shown:

$$\sigma_{(t)} = \frac{P_{(t)}}{A_{(t)}} \quad (17)$$

Then, the creep strain, ε_c , at each time is computed from time, t , temperature, T , and stress, $\sigma_{(t)}$, based on the [Fields and Fields \(1989\)](#) creep model with an additional constant, c_5 , along with unit conversions. Further, the material-specific parameters, a , b and c , are functions of temperatures as shown:

$$\varepsilon_c = 0.01c_5a t^b (145.038\sigma_{(t)})^c \quad (18)$$

$$a = 10^{-(6.1+0.00573T)} \text{ for } T < 500^\circ\text{C} \quad (19)$$

$$a = 10^{-(13.25-0.00851T)} \text{ for } T > 500^\circ\text{C} \quad (20)$$

$$b = -1.1 + 0.0035T \quad (21)$$

$$c = 2.1 + 0.0064T \quad (22)$$

Hooke's law can be used in stress computations, given the elastic behavior of the beam with a Poisson's ratio ν . Thus, the axial stress due to creep, $\sigma_{c(t)}$, is the creep strain, ε_c , multiplied by the modulus, $E_{(t)}$, at the time, t :

Case	C_1 (600 to 500°C)	C_2 (500 to 400°C)	C_3 (400 to 20°C)
LR 33%	1.01	1.003	1.003
LR 50%	1.03	1.005	1.005
LR 67%	1.06	0.98	1.007
Small column	1	1	1
Short column	1.05	0.96	1.006

Table 1.
Summary of the moment constants used in the cooling phase of the fast analysis

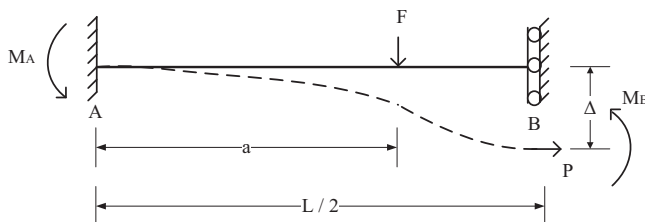


Figure 5.
Catenary action schematic

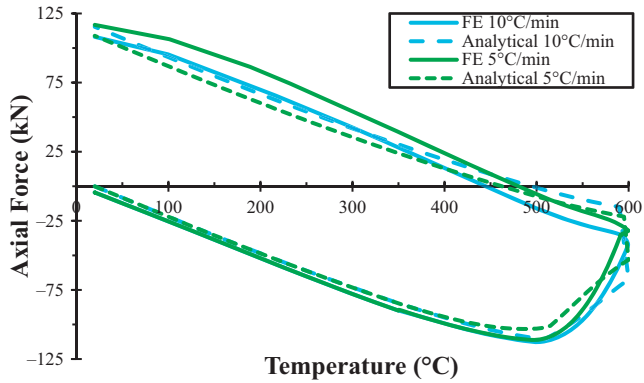
$$\varepsilon_c = \frac{\sigma_x(t)}{E(t)} - \nu \left(\frac{\sigma_y(t)}{E(t)} + \frac{\sigma_z(t)}{E(t)} \right) \quad (23)$$

$$\sigma_c(t) = \varepsilon_c E(t) \quad (24)$$

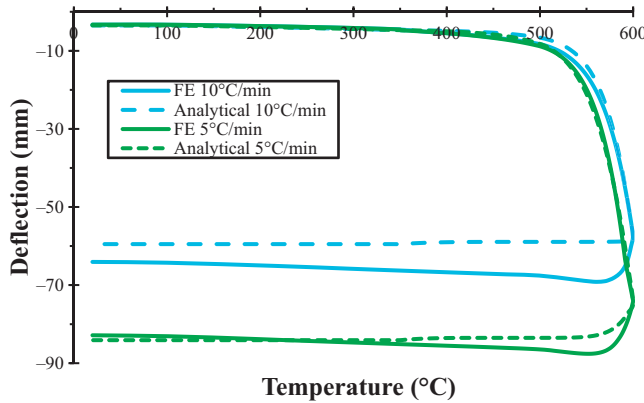
300

Table 2.
Summary of the
creep force and
deflection constants

Case	C ₄ (Δ Heating)	C ₅ (P Cooling)	C ₆ (Δ Cooling)
LR 33%	-0.5	1	-7
LR 50%	2.5	28	1
LR 67%	2.5	28	9
Small column	12	1	30
Short column	-3.5	1	-7
Heating limit 550°C	11	10	0
Heating limit 500°C	11	10	-7



(a)



(b)

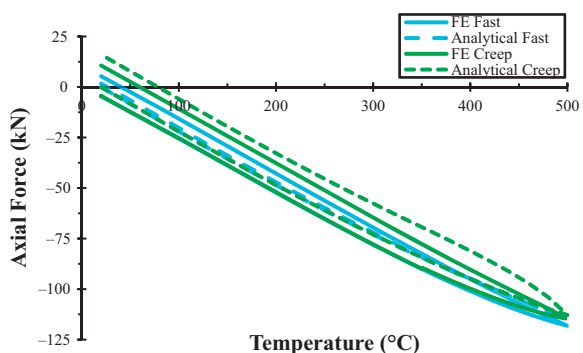
Figure 6.
FE and analytical
results for heating
and cooling rates of 5
and 10°C/min,
respectively,
including creep: (a)
beam axial force; (b)
mid-span deflection

After obtaining the axial stress, the axial force, including creep, is the product of the total stress and the area, where $\sigma_{(t)}$ is the axial stress computed from the fast analysis:

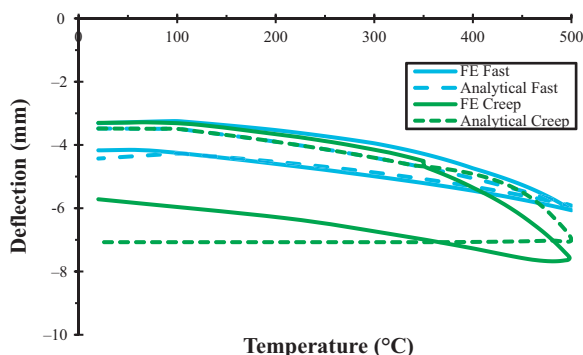
$$P_{(t)} = (\sigma_{c(t)} + \sigma_{(t)})A_{(t)} \quad (25)$$

The deflection considering creep is computed from the deflection of the previous time ($t-1$) multiplied by the ratio of total strain to the strain, excluding creep. Although the stiffness matrices take into account the assembly behavior, creep analysis was performed on a specific area only, which is the beam mid-span. Therefore, creep should be magnified with the help of curve-fitted constants. This magnification was applied using the temperature increment, ΔT , in addition to the creep constants, c_4 and c_6 , for heating and cooling stages, respectively. All the creep constants, c_4 , c_5 and c_6 , are represented in Table 2. The below equation summarizes the computation of the deflection including creep:

$$\Delta_{(t)} = \Delta_{(t-1)} \frac{\varepsilon_{total}}{\varepsilon_{total} - (0.4\Delta T + c_{4,6})\varepsilon_c} \quad (26)$$



(a)



(b)

Figure 7.
FE and analytical
results for 500°C
initial cooling
temperature: (a) beam
axial force; (b) mid-
span deflection

5. Results and discussion

The proposed model is validated against the results of the parametric studies performed by Al Haddad *et al.* (2019). The parametric studies include heating and cooling rates, initial cooling temperatures, load ratios, column sizes and heights. The proposed analytical model starts with the loading phase at ambient 20°C, then is heated up to 600°C (Fields and Fields temperature limit), then follows a linear cooling trend back to 20°C.

5.1 Heating and cooling rates

Heating and cooling rates of 5 and 10°C/min are chosen for this parameter while including creep. As Figure 2 illustrates, a significant drop can be seen in the elastic modulus between 500 and 600°C, approximately to its half. This significant reduction allowed the beam axial force in Figure 6(a) to start increasing at 500°C, forming a peak compressive force of nearly 110 kN. The analytical model axial force shows accurate axial forces when compared to the FE models for rates of 5 and 10°C/min alike. For the beam deflection condition shown in Figure 6(b), the deflection of the analytical model is also very close to those of the FE models. It should be noted that the analytical model is capable of predicting the increase in creep deflections caused by the reduction of rates from 10 to 5°C/min. This behavior is commonly observed in creep studies when steel is exposed to longer durations of heating and cooling.

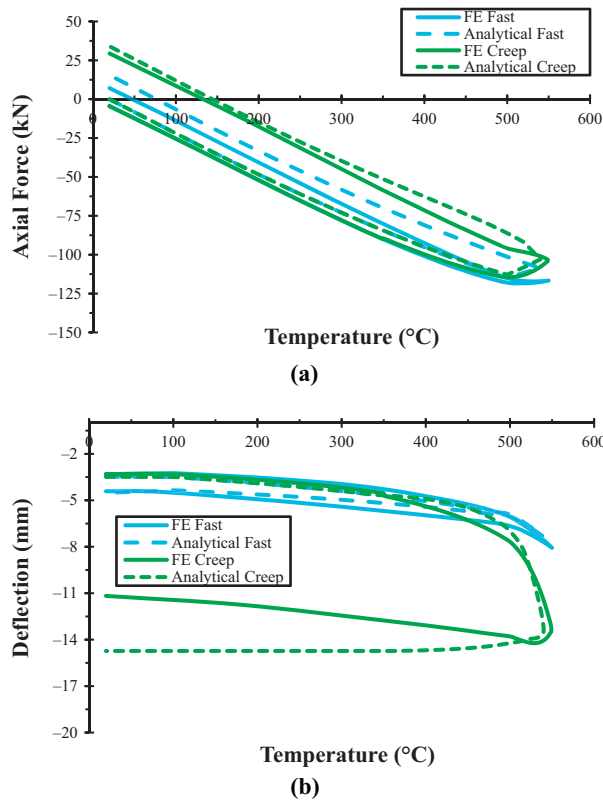


Figure 8. FE and analytical results for 550°C initial cooling temperature: (a) beam axial force; (b) mid-span deflection

5.2 Initial cooling temperature

The initial cooling temperature is the maximum temperature the model has reached before it starts cooling. In this study, the initial cooling temperature is changed from 600°C to 500 and 550°C for both of the fast and creep analyses, respectively. First, it can be clearly observed from Figure 7 that reducing the initial cooling temperature from 600°C to 500°C greatly reduces the difference between the fast and creep analyses regarding both axial forces and deflections. This reduction of the thermal creep effect is less when reducing from 600°C to 550°C, as presented in Figure 8. The main reason for the reduction of creep effect is that creep normally initiates at 350°C and becomes more severe after 500°C. Second, it is evident from Figure 7(b) and 8(b) that the deflections of the fast analytical model during the cooling stage match the FE models much more than the creep analysis. This is due to the deflection decrease observed in the FE models, which is caused by the material strength recovery along with the stress and temperature reductions occurring during cooling. The deflection recovery during the cooling stage could not be observed in the creep analytical model.

5.3 Load ratio

The load ratio is the ratio of the largest beam moment generated because of the imposed loads to the moment plastic capacity of the beam at ambient temperature. The point loads applied in this study are 26.7, 40 and 53.3 kN to achieve 0.33, 0.5 and 0.67 load ratios, respectively. Figures 9, 10 and 11 represent FE and analytical beam axial forces and

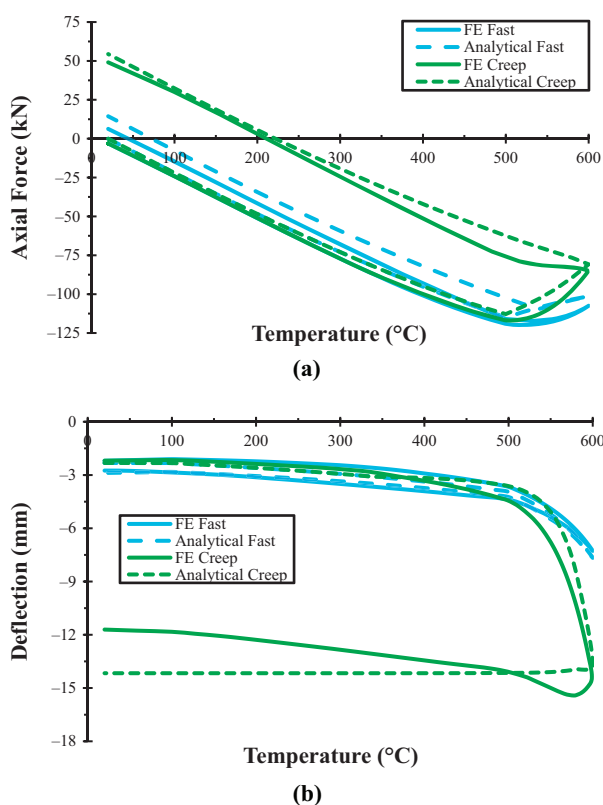


Figure 9.
FE and analytical
results for 33% load
ratio: (a) beam axial
force; (b) mid-span
deflection

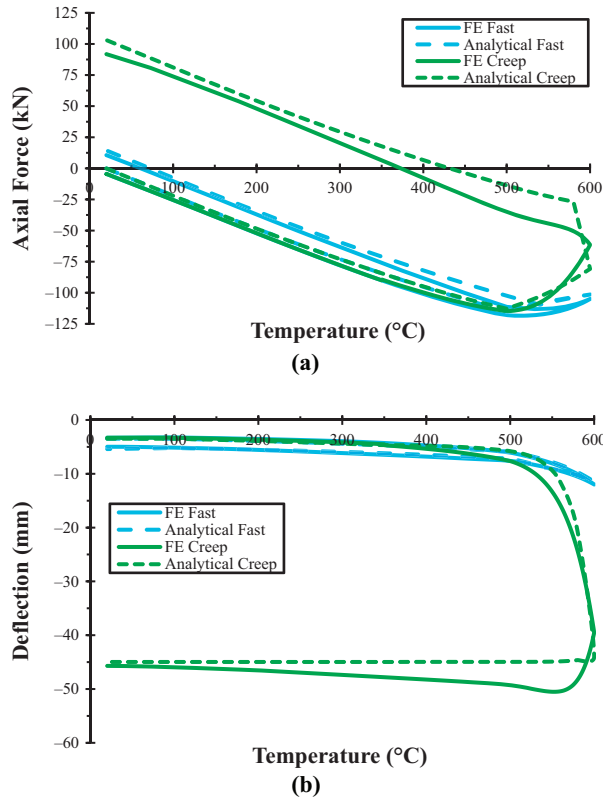


Figure 10.
FE and analytical
results for 50% load
ratio: (a) beam axial
force; (b) mid-span
deflection

deflections versus beam temperatures for the three load ratios with and without creep. It is evident that the analytical model was capable of predicting the results of the FE models. Three main observations should be noted. First, it can be clearly seen that as the load ratios increase, the difference between fast and creep analyses increases. Second, the contact at the end of the heating stage in the FE model, where 0.67 load ratio is applied, could not be modeled in the analytical model. Third, the sudden axial force change in the three creep analytical model cases at the start of cooling is caused by the application of the constant, c_5 . This constant was used because creep analysis is based on the mid-span area only, and the creep analysis approach between two times was incremental, starting with very small axial forces at the start of cooling as shown in [Figures 9\(a\), 10\(a\) and 11\(a\)](#).

5.4 Column size

The column cross-section affects the flexural stiffness of a column, which highly influences the axial restraint imposed on the beam. Instead of the regular UC $254 \times 254 \times 73$ section used in all other cases, a smaller UC $152 \times 152 \times 23$ column size was used for fast and creep cases. It should be noted that the smaller column is made up of S275 in the experiment, so S275 was also used in the FE and analytical simulations. The smaller column section applied less beam axial restraint, thereby reducing the beam axial forces greatly for both fast and creep cases, as can be seen in [Figure 12\(a\)](#). The beam axial force in the analytical

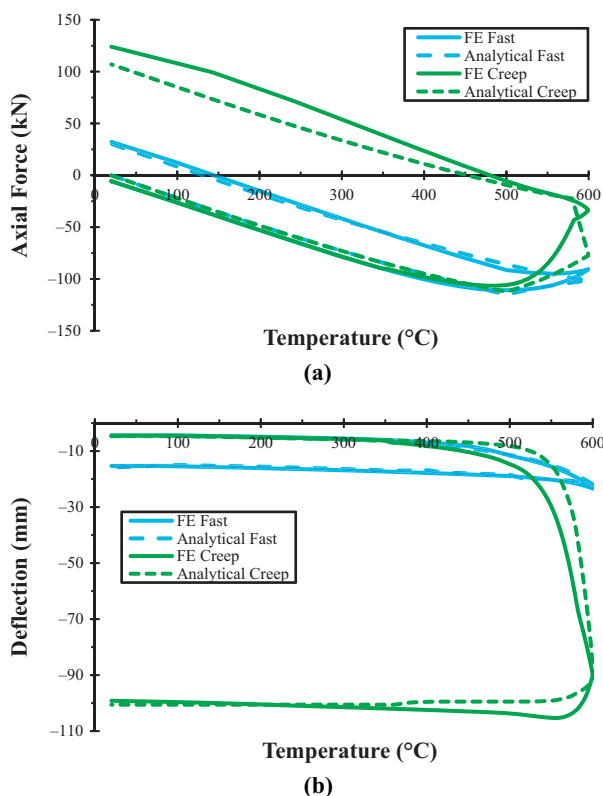


Figure 11.
FE and analytical
results for 67% load
ratio: (a) beam axial
force; (b) mid-span
deflection

model shows a maximum deviation of around 3 kN from the FE results, a small difference that is magnified graphically due to the small maximum force reached in the FE model (about 15 kN only). The same can be said regarding beam deflections, as shown in Figure 12(b), which indicates that the analytical model predicted the FE results accurately for the small column case. A final note on the beam deflection of the fast case is that it is identical during heating and cooling stages, which is mainly the result of the extremely small stresses encountered causing a full-deflection recovery in the beam.

5.5 Column height

In spite of its great impact on beam axial restraint, the column height is not included in previous analytical and mechanical models. The columns considered in this analysis are also UC $254 \times 254 \times 73$ sections but with a 2.45 m height instead of the 3.67 m used for all other cases. The 400 mm heated region of the column is the same in all cases. Due to the additional axial restraint, huge axial forces can be observed from Figure 13(a), which are almost double the forces when compared to longer columns. Further, because of the large stresses developed at the early stages of heating, the maximum compressive load is observed at 350°C instead of the previously observed 500°C.

When creep was included in the FE model, beam and column flange contact occurred at the end of the heating stage. As discussed before, the analytical model could not predict

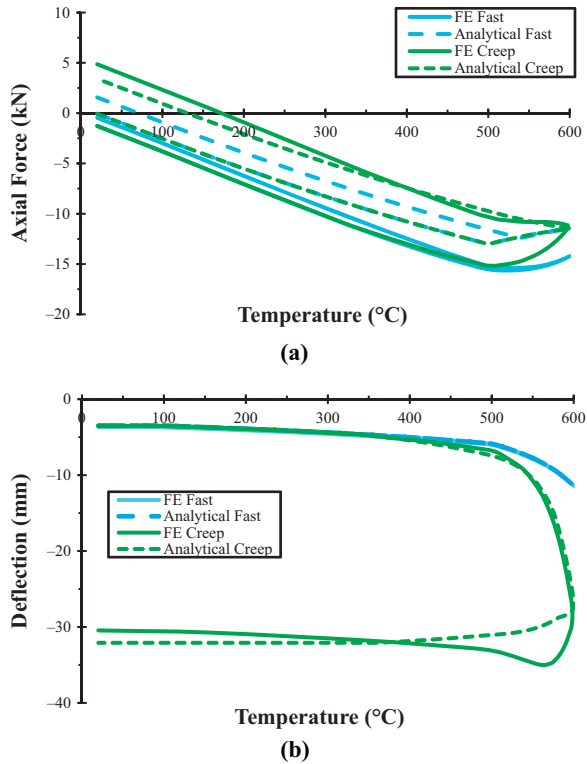


Figure 12.
FE and analytical
results for small
column size: (a) beam
axial force; (b) mid-
span deflection

contact, but was able to predict the shear endplate yielding observed in the FE fast and creep models at the end of the cooling phase. The shear endplate yielding can be observed from the nearly constant axial force growth in [Figure 13\(a\)](#). In addition, beam web and top flange yielding was observed in the FE models just after 350°C, which was also predicted by the analytical model as can be observed in the deflection presented in [Figure 13\(b\)](#). The deflection rapidly increases after 350°C, with more significance in the creep model compared to the fast model. Therefore, the column height parameter was reasonably modeled analytically regarding axial forces, deflections and yielding of the beam and endplate.

6. Conclusions

This study summarizes the analytical modeling of the transient state creep behavior of shear endplate connection assemblies. The analytical model has proven its capability of predicting the strength and deformation of the beam-column assembly when compared with the FE results.

The analytical model is able to predict, with reasonable accuracy, the beam axial forces and mid-span deflections for different fire scenarios. More specifically, the analytical model shows the significance of thermal creep effect on the behavior of the shear endplate assembly as exposed to longer fire durations.

The analytical model results show that the beam deflection and axial stress relaxation are significant for high temperatures and stresses when the thermal creep effect is

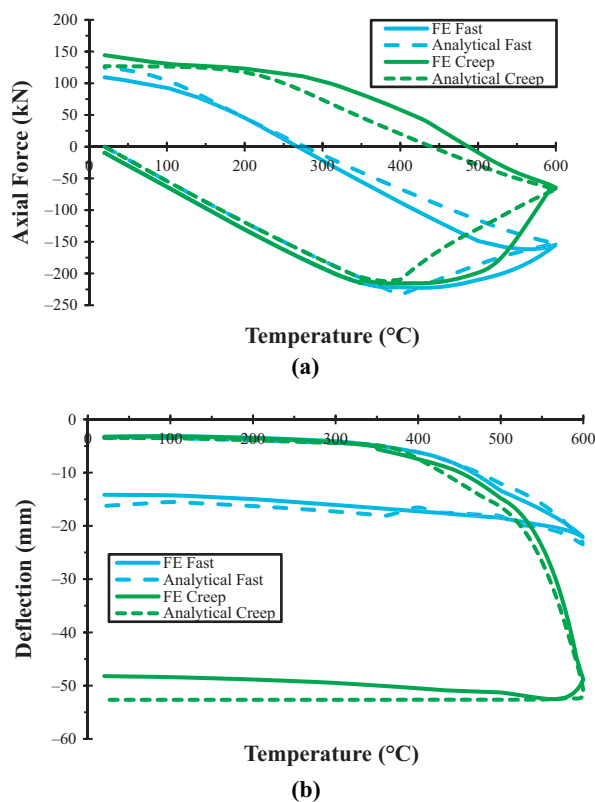


Figure 13.
FE and analytical
results for short
column height: (a)
beam axial force; (b)
mid-span deflection

considered. Also, the results show that when creep is considered explicitly in the analysis, the beam undergoes excessive deformation. This deformation needs to be taken into account in the design to guarantee the structural integrity of steel buildings when exposed to fire.

The analytical model presents several benefits when compared to the experimental tests and numerical simulations. The analytical model requires less computational efforts when compared to FE models. In addition, the proposed analytical model can be considered as a practical tool for design engineers to use.

Several enhancements can be applied on the proposed analytical model to increase its accuracy. The first limitation is the constants used in the analytical model. These constants are limited to shear endplate connections having the material and geometrical parameters specified in this study. To use the analytical model for other types of connections and configurations, more generalized equations for these constants need to be developed. The second limitation is the prediction of the mid-span deflection recovery for cases where creep is considered. Therefore, more research work is needed to account for this limitation to have a better prediction of the deflection during the cooling phase of a fire event. Further, the proposed model can be improved to predict the beam axial force after beam-column contact. This improvement can be applied by setting a certain rotation limit, which when reached, the beam stiffness increases to account for the additional stiffness gain by contact. However,

to estimate the rotational limit and the adjusted beam stiffness accurately, more investigations should be conducted on the connection level for accurate contact predictions. Finally, because the tertiary stage cannot be modeled using [Fields and Fields \(1989\)](#) creep model, it was not included in this study. However, more reliable creep models need to be developed to compute thermal creep strains at the tertiary stage.

References

- ABAQUS (2014), *Ver. 6.14 Documentation*, Dassault Systemes Simulia Corporation, Waltham.
- Al Haddad, H.O., Hantouche, E.G. and Al Khatib, K.K. (2019), "Numerical studies on the creep behavior of shear endplate connection assemblies under transient heating", *Fire Technology*, Vol. 55 No. 6, pp. 2341-2367.
- Al-Jabri, K.S., Burgess, I.W. and Plank, R.J. (2005), "Spring-stiffness model for flexible end-plate bare-steel joints in fire", *Journal of Constructional Steel Research*, Vol. 61 No. 12, pp. 1672-1691.
- Block, F.M. (2006), *Development of a component-based finite element for steel beam-to-column connections at elevated temperatures*, ProQuest Dissertations Publishing.
- El Ghor, A.H. and Hantouche, E.G. (2017), "Thermal creep mechanical-based modeling for flush endplate connections in fire", *Journal of Constructional Steel Research*, Vol. 136, pp. 11-23.
- Fields, A.B. and Fields, J.R. (1989), *Elevated temperature deformation of structural steel*, National Institute of Standards and Technology (NIST), Gaithersburg, MD.
- Hantouche, E.G. and Sleiman, S.A. (2017), "Axial restraint forces in shear endplates of steel frames due to fire", *Journal of Constructional Steel Research*, Vol. 128, pp. 528-541.
- Hantouche, E.G., Al Khatib, K.K. and Morovat, M.A. (2018), "Modeling creep of steel under transient temperature conditions of fire", *Fire Safety Journal*, Vol. 100, pp. 67-75.
- Hantouche, E.G., Jabotian, H.V., Al Khatib, K.K., El Ghor, A.H. and Morovat, M.A. (2018), "A Unified Mechanical Model for Fire Design of Simple Steel Connections", *Structures Congress 2018*, pp. 140-150.
- Harmathy, T.Z. (1967), "A Comprehensive Creep Model", *Journal of Basic Engineering*, Vol. 89 No. 3, p. 496.
- Hu, Y., Davison, B.J., Burgess, W.I. and Plank, R.J. (2007), "Comparative Study of the behaviour of BS 4190 and BS EN ISO 4014 bolts in fire", *3rd International Conference on Steel and Composite Structures*, Taylor and Francis, Manchester, p. 587.
- Hu, Y., Davison, B., Burgess, I. and Plank, R. (2009), "Component modelling of flexible end-plate connections in fire", *International Journal of Steel Structures*, Vol. 9 No. 1, pp. 1-15.
- Jabotian, H.V. and Hantouche, E.G. (2018), "Thermal creep effect on the behavior of shear tab connections due to fire temperatures", *Fire Safety Journal*, Vol. 96, pp. 74-92.
- Jaspart, J. Weynand, K. and Steenhuis, M. (1995), "The stiffness model of revised Annex J of Eurocode 3".
- Kodur, V. and Dwaikat, M. (2010), "Effect of high temperature creep on the fire response of restrained steel beams", *Materials and Structures*, Vol. 43 No. 10, pp. 1327-1341.
- Lee, J., Morovat, M.A., Hu, G., Engelhardt, M.D. and Taleff, E.M. (2013), "Experimental investigation of mechanical properties of ASTM A992 steel at elevated temperatures", *Engineering Journal*, Vol. 50 No. 4, pp. 249-272.
- Luecke, W.E., McColskey, J.D., McCowan, C.N., Banovic, S.W., Fields, R.J., Foecke, T.J., Siewert, T.A. and Gayle, F.W. (2005), "Federal Building and Fire Safety Investigation of the World Trade Center Disaster: Mechanical Properties of Structural Steels", Report NIST NCSTAR 1-3D, National Institute of Standards and Technology, Gaithersburg, MD.

- Morovat, M.A. (2014), "Creep buckling behavior of steel columns subjected to fire", Ph.D. Dissertation, Department of Civil, Architectural and Environmental Engineering, The University of TX at Austin.
- Sarraj, M. (2007), *The Behaviour of Steel fin Plate Connections in Fire*, ProQuest Dissertations Publishing.
- Spyrou, S., Davison, J.B., Burgess, I.W. and Plank, R.J. (2004), "Experimental and analytical investigation of the 'tension zone' components within a steel joint at elevated temperatures", *Journal of Constructional Steel Research*, Vol. 60 No. 6, pp. 867-896.
- Torić, N. and Burgess, I.W. (2016), "A unified rheological model for modelling steel behaviour in fire conditions", *Journal of Constructional Steel Research*, Vol. 127, pp. 221-230.
- Torić, N., Harapin, A. and Boko, I. (2013), "Modelling of Steel Creep at High Temperatures Using an Implicit Creep Model", *Key Engineering Materials*, Vol. 553, pp. 13-22.
- Wang, Y.C., Dai, X.H. and Bailey, C.G. (2011), "An experimental study of relative structural fire behaviour and robustness of different types of steel joint in restrained steel frames", *Journal of Constructional Steel Research*, Vol. 67 No. 7, pp. 1149-1163.
- Wang, W., Yan, S. and Liu, J. (2017), "Studies on temperature induced creep in high strength Q460 steel", *Materials and Structures*, Vol. 50 No. 1, pp. 1-14.
- Yang, K. and Yu, Z. (2013), "Experimental research on the creep buckling of fire-resistant steel columns at elevated temperature", *Steel and Composite Structures*, Vol. 15 No. 2, pp. 163-173.

Further reading

- European Committee for Standardization (2005), "Eurocode 3: design of steel structures- Part 1-8: Design of joints and building frames", BS EN 1993-1-8, Brussels.
- National Institute of Standards and Technology (2005), Final Report on Collapse of the World Trade Center Towers, Washington, DC.

Corresponding author

Elie G. Hantouche can be contacted at: eh12@aub.edu.lb

For instructions on how to order reprints of this article, please visit our website:

www.emeraldgrouppublishing.com/licensing/reprints.htm

Or contact us for further details: permissions@emeraldinsight.com